2005

The Cluster-Scale AGN Outburst in Hydra A

P. Nulsen
University of Wollongong

B. R. McNamara
Ohio University, USA

M. W. Wise
Massachusetts Institute of Technology, USA

L. P. David
Harvard-Smithsonian Center for Astrophysics, Cambridge, USA

The Astrophysical Journal, 628:629–636, 2005 August 1

THE CLUSTER-SCALE AGN OUTBURST IN HYDRA A

P. E. J. Nulsen,[1,2] B. R. McNamara,[3] M. W. Wise,[4] and L. P. David[1]
Received 2004 August 12; accepted 2005 April 10

ABSTRACT

Deep *Chandra* observations of the Hydra A Cluster reveal a feature in the X-ray surface brightness that surrounds the 330 MHz radio lobes of the AGN at the cluster center. Surface brightness profiles of this feature and its close association with the radio lobes argue strongly that it is a shock front driven by the expanding radio lobes. The *Chandra* image also reveals other new structure on smaller scales that is associated with the radio source, including a large cavity and filament. The shock front extends 200–300 kpc from the AGN at the cluster center, and its strength varies along the front, with Mach numbers in the range ∼1.2–1.4. It is stronger where it is more distant from the cluster center, as expected for a shock driven by expanding radio lobes. Simple modeling gives an age for the shock front of $\sim 1.4 \times 10^8$ yr and a total energy driving it of $\sim 10^{61}$ ergs. The mean mechanical power driving the shock is comparable to quasar luminosities, well in excess of that needed to regulate the cooling core in Hydra A. This suggests that the feedback regulating cooling cores is inefficient, in that the bulk of the energy is deposited beyond the cooling core. In that case, a significant part of cluster "preheating" is a by-product of the regulation of cooling cores.

Subject headings: cooling flows — galaxies: active — galaxies: clusters: individual (Hydra A) — intergalactic medium — X-rays: galaxies: clusters

1. INTRODUCTION

The X-ray–emitting gas at the centers of many cooling flow clusters is cooler than the surrounding gas and has cooling times in the range 10^8–10^9 yr. Despite this, little of the gas cools below ∼1 keV (e.g., Peterson et al. 2001, 2003; Tamura et al. 2001; Kaastra et al. 2004). The main issue for cooling flows has become that of determining what heat source makes up for radiative losses from the gas. Many possibilities have been proposed, including thermal conduction (e.g., Narayan & Medvedev 2001), energy released by mergers (e.g., Motl et al. 2004), and heating by an active galactic nucleus (AGN; Tabor & Binney 1993; Tucker & David 1997). However, maintaining gas for many cooling times, while preventing it from cooling to low temperatures or being heated until its cooling time is comparable to its age, requires a fine balance between heating and cooling. Since cooling flows are common (Fabian 1994), they cannot be a transient phenomenon, and plausible mechanisms for maintaining the gas with short cooling times must almost certainly involve feedback. While they face some difficulties (e.g., Fabian et al. 2001), AGN heating models provide a natural feedback mechanism, making them the strongest candidate to solve this cooling flow problem.

There is clear evidence for some AGN heating in cooling flows. Large galaxies are prevalent at cluster centers, and Burns (1990) has shown that cD galaxies at the centers of cooling flows have a high incidence of radio activity. High-resolution X-ray images reveal that radio lobes fed by AGNs have created cavities in the hot gas in a growing number of clusters (Böhringer et al. 1993; Carilli et al. 1994; McNamara et al. 2000, 2001; Fabian et al. 2000; Blanton et al. 2001; Schindler et al. 2001; Heinz et al. 2002; Young et al. 2002) and also in the hot interstellar medium of individual elliptical galaxies (Finoguenov & Jones 2001; Kraft et al. 2004). Churazov et al. (2002) pointed out that the enthalpy of a cavity (bubble) can be thermalized as it rises buoyantly, providing a heat source for the gas. Simple arguments show that the enthalpy is thermalized in the wake of a rising bubble, provided that the bubble is not too large compared to its distance from the cluster center (Birzan et al. 2004). Using optimistic estimates for the heating rate, Birzan et al. (2004) analyzed data for all cavities that they could identify in the *Chandra* archive and found that, while the heating rate due to bubbles can be significant, it typically falls several times short of radiative losses.

Standard models of jet-fed radio lobes (e.g., Scheuer 1974; Heinz et al. 1998) posit the existence of a "cocoon shock" that surrounds the rapidly expanding radio lobes. Although there is commonly a bright rim around the radio lobe cavities in X-ray clusters, this is composed of cool (low entropy) gas, close to local pressure equilibrium (e.g., Nulsen et al. 2002), so most cavities are not strongly overpressured (Cen A is a noteworthy exception; Kraft et al. 2003). However, evidence has begun to emerge for weak shocks generated by the radio lobes in cooling flows. Fabian et al. (2003) found ripples in the surface brightness of the Perseus cluster, which they interpret as weak shocks (sound waves) generated as the expansion rate of the lobes varies. They argue that heating due to viscous dissipation of sound can make up for radiative losses from the Perseus cooling flow. This process has been simulated by Ruszkowski et al. (2004). Young et al. (2002) found a weak shock surrounding M87 in the Virgo Cluster, and Forman et al. (2005) found evidence of further shocks in a deeper X-ray image. They determined the energy of the outburst that drove the best-defined shock, using the result to show that heating due to weak shocks is sufficient to stop the cooling flow in M87.

Here we report the discovery of a weak shock front generated by an AGN outburst in the Hydra A Cluster. Hydra A has well-known radio lobe cavities (McNamara et al. 2000; David et al. 2001; Nulsen et al. 2002), which surround the 1.4 GHz inner radio lobes and extend to ∼40″ (40 kpc) from the cluster center.

[1] Harvard-Smithsonian Center for Astrophysics, 60 Garden Street, Cambridge, MA 02138.
[2] On leave from the University of Wollongong.
[3] Astrophysical Institute and Department of Physics and Astronomy, Clippinger Laboratories, Ohio University, Athens, OH 45701.
[4] Center for Space Research, Building NE80-6015, Massachusetts Institute of Technology, Cambridge, MA 02139.

By contrast, the weak shock front discussed here extends up to $\sim 6'$ from the cluster center, surrounding the much larger low-frequency radio lobes (Lane et al. 2004) and representing a much more energetic phenomenon.

In § 2 we give details of the observations and data reduction. In § 3 we discuss the main features of the new deep image of Hydra A, and in § 4 we discuss the evidence for the shock front and estimate the energy of the outburst that drove it. The implications of this shock for cooling flows and clusters in general are discussed in § 5. We assume a flat ΛCDM cosmology, with $H_0 = 70$ km s^{-1} Mpc^{-1} and $\Omega_m = 0.3$, giving a scale of 1.05 kpc arcsec^{-1} at the redshift of Hydra A, $z = 0.0538$.

2. OBSERVATIONS AND DATA REDUCTION

Hydra A was observed with *Chandra* for 98.2 ks on 2004 January 13, with ACIS-S at the aim point in VFAINT mode (ObsID 4969). A *z*-sim offset of 5 mm was used to keep the cluster center close to the optical axis, while extending the field of view to the north to cover the northern low-frequency radio lobe (Lane et al. 2004). The event list was screened to remove *Advanced Satellite for Cosmology and Astrophysics* (*ASCA*) grades 1, 5, and 7, and bad pixels in the standard manner. A large background flare made it necessary to set the mean background count rate manually when using `lc_clean` to remove periods of high particle background, but the mean count rate in ACIS S1 after cleaning is close to the expected value.[5] After cleaning, 66.4 ks of good data were left. The data were processed to correct for time dependence of the ACIS gain.[6] Data were filtered according to the prescription of Vikhlinin[7] to reduce particle background. Background event files were created by processing the standard ACIS background files in the same manner as the data. Point sources were identified manually for removal from spectra and surface brightness profiles. When extracting spectra, ancillary response functions (ARFs) and redistribution matrix files (RMFs) for extended regions are weighted by the number of events in each subregion. ARFs are corrected to allow for the reduction in low-energy response due to the build-up of contaminants on the ACIS filters.

3. X-RAY STRUCTURE OF HYDRA A

Figure 1 shows a background-subtracted, exposure-corrected, and smoothed image of Hydra A in the 0.5–7.5 keV band. The exposure correction assumes an absorbed MEKAL spectrum, with the foreground column density $N_{\rm H} = 4.94 \times 10^{20}$ cm^{-2}, temperature $kT = 4$ keV, abundances of 0.3 times solar, and a redshift of 0.0538. In order to make structures visible over a wide range of radius, the image has been divided by a spherical beta model, with a core radius of $98''$, with $\beta = 0.6$ and centered on the AGN. The field is covered by ACIS S3 and part of S2 (to the northeast). For scale, the chips are $8\farcm4$ wide. The southwest cavity of McNamara et al. (2000) can be seen $\sim 0\farcm5$ to the southwest of the bright AGN. The corresponding radio cavity to the northeast is also visible, although less clearly defined. A $\sim 1'$ bright filament stretches from the inner cavity to about the center of a larger outer cavity in the northeast (cavity C). The association between the $1'$ bright filament to the northeast and the radio jet of Hydra A is reminiscent of the southwest filament in M87 (Forman et al. 2005), suggesting a similar origin. The filament in Hydra A is roughly twice as long as that in M87, but the radio source in Hydra A is a lot larger too. Cavity C has a radius $\sim 0\farcm6$ (40 kpc) and occurs at the sharp bend in the radio jet leading to the northern 330 MHz radio lobe (see Fig. 2). There is also a deficit in the X-ray emission $\sim 2'$ to the southwest of the AGN, associated with the southern 330 MHz radio lobe.

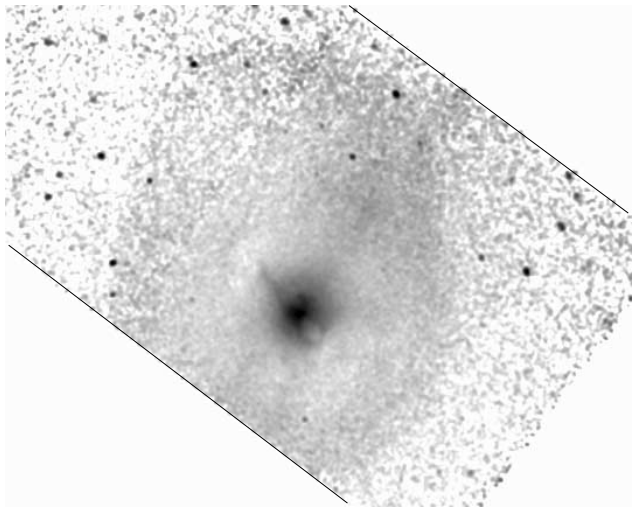

FIG. 1.—*Chandra* 0.5–7.5 keV image of Hydra A. The image from the S2 and S3 chips has been background-subtracted, exposure-corrected, smoothed with a $2''$ Gaussian, and divided by a spherical beta model centered on the AGN. The distance between the edges of the chips (marked by lines running from northeast to southwest across the image) is $8\farcm4$. The cavities of McNamara et al. (2000) can be seen close to the bright AGN. The cavity $1'$–$2'$ northeast of the AGN (cavity C), at the end of the bright filament, occurs where the 330 MHz radio jet bends sharply to the northwest (see Fig. 2). The shock front surrounding the radio lobes of Fig. 2 is visible, particularly to the east and north.

There is an edge in X-ray surface brightness, running from $\sim 4\farcm3$ east to $\sim 6'$ north of the AGN, that continues around the AGN. The northern part of this edge was noted previously by Forman et al. (2000) and by Markevitch et al. (2003). Although it is less distinct to the west, this feature can be traced all the way around the AGN, except where it falls off the detectors in the south. We interpret the feature as a shock front and refer to it this way from here on. Figure 2 shows the same X-ray image as Figure 1, together with contours of the 330 MHz radio map of Lane et al. (2004). The northern radio lobe lies close inside the northern part of the shock front and has a similar shape. Although the X-ray image of the shock front is truncated to the south, enough of it is visible to see that, along with the 330 MHz radio lobe, it lies closer to the AGN in the south. The correspondence between the shapes of the radio lobes and the shock front supports the interpretation of this surface brightness feature as a shock front driven by the outburst that formed the radio lobes.

4. SHOCK MODELS FOR HYDRA A

4.1. *Shock Brightness Profiles*

Figure 3 (*top*) shows the surface brightness profile of the region to the west of Hydra A, in a sector centered on the AGN, from position angle (P.A.) 240° to 300°. Point sources were eliminated, the background was subtracted, and the resulting profile was exposure corrected. The abrupt change in slope at a radius of $202''$ (211 kpc) is due to the feature that we identify as a shock. Outside this, the surface brightness is well fitted by the power law $r^{-\alpha}$ with $\alpha = 2.65 \pm 0.17$ (90% confidence). A surface brightness profile was also extracted in the region to the northeast of

[5] See http://cxc.harvard.edu/contrib/maxim/acisbg/data/README.
[6] See http://hea-www.harvard.edu/~alexey/acis/tgain.
[7] See http://cxc.harvard.edu/cal/Acis/Cal_prods/vfbkgrnd.

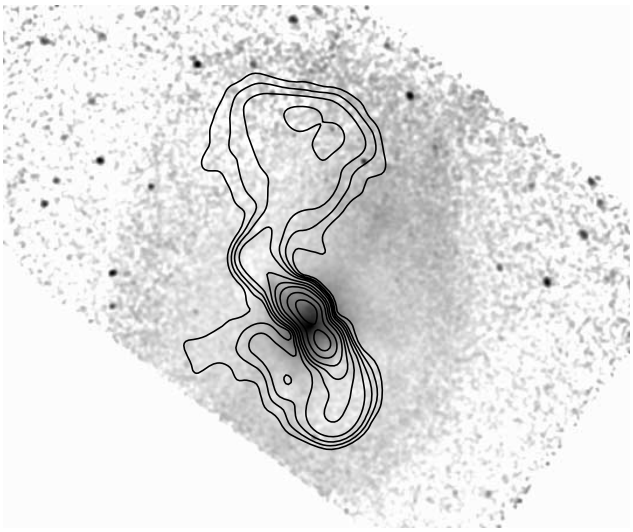

FIG. 2.—X-ray image of Hydra A with 330 MHz radio contours. The image of Fig. 1 is shown with logarithmically spaced contours from the 330 MHz radio map. The two closed contours near the center of the map are at the position of the 1.4 GHz radio lobes, marking the locations of the inner X-ray cavities that can be seen in Fig. 1.

the AGN, where the edge in the surface brightness is most prominent. This is shown in Figure 3 (*bottom*). In order to match the curvature of the radial bins to that of the front, the sector was centered at a point approximately 2.′9 north of the AGN (at R.A. = $9^{h}18^{m}7^{s}.30$, decl. = $-12^{\circ}2'48''.4$ [J2000.0]), with the range of P.A. $20^{\circ}-70^{\circ}$. Although the data are noisy, the edge is evident in the surface brightness profile at a radius of about 200″ (measured from the center of the sector).

The break in surface brightness in the northeast is greater than that in the west, showing that the shock is stronger in the northeast. This is consistent with expectations for radio lobe–driven shocks. Shock strength is determined by the ratio of postshock to preshock pressure. The preshock pressure is significantly lower in the north, where the shock is farthest from the cluster center. To a first approximation, the pressure rise behind the shock is uniform around the front (assuming that jet momentum is insignificant on such large scales). Thus, the pressure jump is greater at points on the shock front that are farther from the cluster center.

The shock front lies ∼3.′4 west of the AGN and ∼4.′3 to the east, implying a significant east-west asymmetry in shock speed. This is most likely due to asymmetry in the medium carrying the shock (as opposed to the outburst driving it) and is probably the result of higher gas density to the west. If the cluster were spherically symmetric, the shock front would be running through denser gas in the west than in the east. Any preexisting density asymmetry that slowed the propagation of the shock to the west would augment this density difference. If postshock pressure is much the same in the east and west, then the shock would be weaker in the west, where it propagates through higher pressure gas. The western shock also appears superimposed on a higher "background" of emission from undisturbed cluster gas. Together, these effects make the shock less distinct in the X-ray image to the west than in that to the east, but it is clearly visible in Figure 3 (*top*).

4.2. *Hydrodynamic Models*

Our aim is to determine the age and energy of the AGN outburst by comparing models to the data. The general form of the radio source in Hydra A is broadly consistent with twin jet models of radio sources (Scheuer 1974). For our purpose, the most important property of the jets is that they convey energy from the AGN into the intracluster medium (ICM). This may be augmented by other forms of AGN energy deposition (e.g., Böhringer & Morfill 1988; Ciotti & Ostriker 2001). Realistic jet models require expensive numerical simulations (e.g., Reynolds et al. 2001; Krause 2004). However, as shown below, the shock is weak and, at least crudely, spherical. In these circumstances the strength of the shock is determined largely by the total energy injected by the AGN. To the extent that the shock front is spherical, the precise location and detailed history of energy injection are of secondary significance. Thus, we use a spherically symmetric model of a point explosion at the center of an initially isothermal, hydrostatic atmosphere to quantify the outburst and shock. The effects of this approximation on our results are discussed further in the next section. Our numerical, hydrodynamic code uses a second-order, Lagrangian spatial differencing scheme and a semi-implicit, second-order time step. It was tested, in particular, to ensure that it reflects the shock jump conditions well. The gas is treated as nonrelativistic (adiabatic index $\gamma = 5/3$), since only a tiny mass of gas gets close to being relativistic in the simulation, and then only briefly.

The radiative cooling time of the central gas $\simeq 4 \times 10^{8}$ yr, about 3 times the age of the shock, so that radiative cooling is ignored. For the shock front in the west, the initial gas density profile is assumed to be a power law, $\rho(r) \propto r^{-\eta}$, with $\eta = 1.82$, which makes the surface brightness profile of the undisturbed gas consistent with the observed surface brightness profile beyond the shock (see above). The gravitational field ($g \propto 1/r$) and gas temperature are scaled to make the undisturbed atmosphere hydrostatic. Surface brightness profiles are determined from the model, assuming that the temperature of the unshocked gas is 4 keV. The *Chandra* 0.6–7.5 keV response was computed using XSPEC, with detector response files appropriate for these observations and an absorbed MEKAL model. The foreground column density was set to 4.94×10^{20} cm^{-2}, the redshift to 0.0538, and the abundance to 0.3 times solar, as appropriate for Hydra A (results are insensitive to these parameters, including the preshock temperature). The shock weakens as the hydrodynamic model evolves, and, since the initial conditions are self-similar, the flow can be scaled radially to place the model shock at the location of the observed shock. Surface brightness is scaled to match the observed profile in the unshocked region.

The three lines in Figure 3 (*top*) show model surface brightness profiles for shocks with Mach numbers of 1.15, 1.19, and 1.23 (increasing upward). A Mach 1.2 shock gives a reasonably good fit to the observed shock profile to the west. Models were also constructed for the shock to the northwest. Here the preshock density profile is flatter, requiring an initial density power law $\eta = 1.37$ (largely because the shock does not propagate radially in the cluster). Model surface brightness profiles are shown in Figure 3 (*bottom*) for Mach numbers of 1.26, 1.34, and 1.42. The Mach number of the shock to the northeast ∼1.3–1.4, again confirming that the shock is stronger in the northeast than in the west.

Our simple hydrodynamic model is not accurate well behind the shock. The initial density profile is only well approximated as a power law locally. The shock front is clearly aspherical. The outer radio lobes lie close behind the shock front, so that they still have an influence in driving the shock (if not, they would have been left behind the rapidly moving front), violating our assumption that the shock front is driven by a point explosion. However, since the lobes are not close to the shock front everywhere,

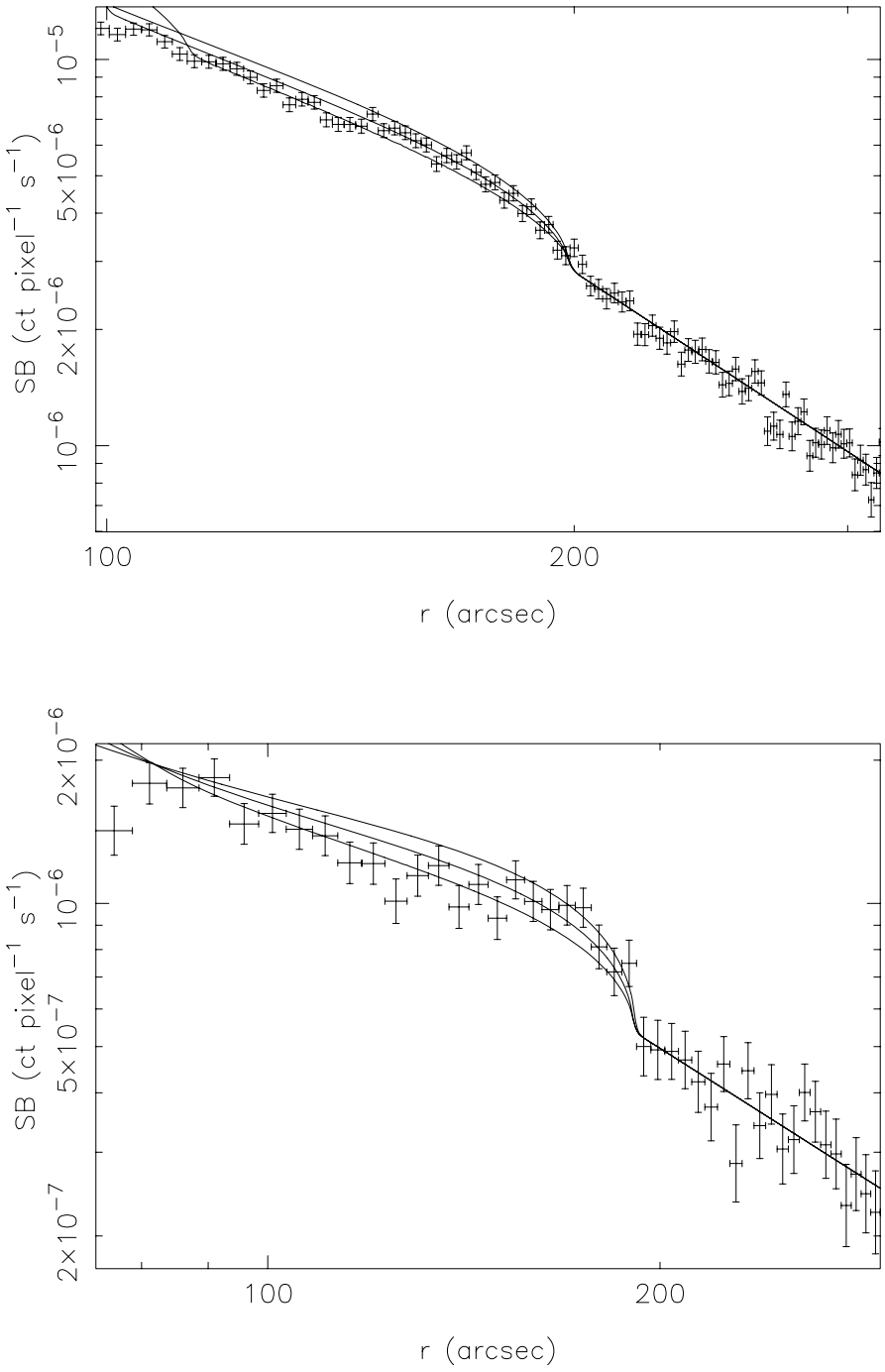

FIG. 3.—Surface brightness profiles of the shock front in Hydra A. *Top*: Radial surface brightness profile measured in the sector from P.A. 240° to 300°, to the west of the AGN, and in the energy range 0.6–7.5 keV. Surface brightness errors are 1 σ statistical errors. Radial error bars show the limits of the bins. The smooth curves show surface brightness profiles for shock models with Mach numbers of 1.15, 1.19, and 1.23, from bottom to top. Models are scaled to match the observed surface brightness outside the shock. *Bottom*: Surface brightness profile at 0.6–7.5 keV of the shock front in the northeast, measured in a sector from P.A. 20° to 50° and centered 2.′9 north of the AGN. Models are shown for shocks with Mach numbers of 1.26, 1.34, and 1.42.

it would also be necessary to drop our assumption of spherical symmetry to make significantly more accurate models. Because of this, the added complexity of models with energy fed continuously into the center of the flow is not warranted. Despite these shortcomings, the models do provide reasonable fits to the surface brightness in the region of the shock front. In particular, they give reasonably accurate measures of the Mach number (the main source of uncertainty is the assumption, implicit in the spherical model, that we know the curvature of the front along the line of sight).

4.3. *Physical Parameters of the Shock*

We base our estimates of outburst age and energy on the model for the western shock, since the assumptions of spherical symmetry and a point explosion are more appropriate in this region. The age and energy of the model outburst depend on the

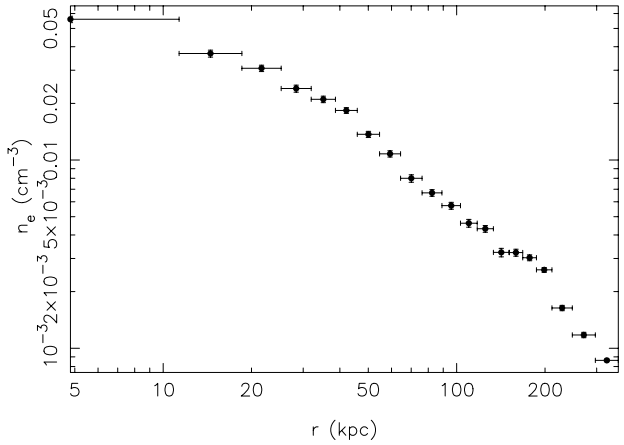

FIG. 4.—Western electron density profile of Hydra A, showing the deprojected electron density vs. radius in the sector from P.A. 240° to 300°. The shock jump is at 211 kpc. Density error bars are 90% confidence ranges, but some are hidden by the data point.

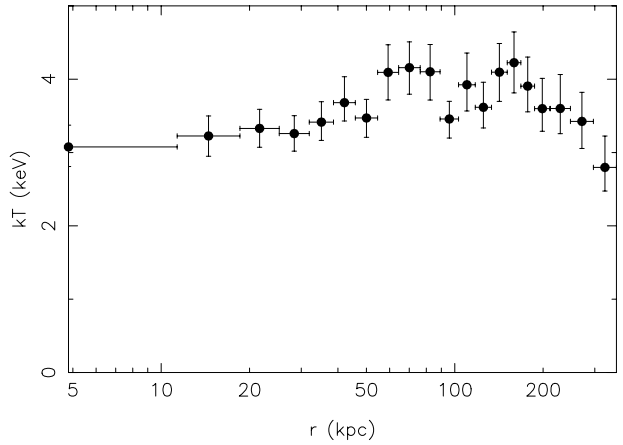

FIG. 5.—Western temperature profile of Hydra A, showing the projected temperature vs. radius in the sector from P.A. 240° to 300°. Error bars show 90% confidence ranges for the temperature.

temperature and density of the unshocked gas, which we determine by deprojection. The sector to the west of the AGN, in which the surface brightness profile in Figure 3 (*top*) was measured, was divided into annular regions having at least 4000 source counts in the 0.6–7.5 keV band. One boundary was fixed at the radius of the shock and others fitted around this in order to avoid smoothing across the shock. Spectra extracted from these regions were used for the deprojection. The method is essentially as described in David et al. (2001). The spectral model for each ring (annular region) includes components for all outer shells, as well as the current one. Only model parameters for the current shell are varied when fitting a ring, so parameters for each spherical shell are determined in turn, working inward. The model component for each outer shell is weighted by the ratio of the volumes of the intersections between that shell, and the current and outer rings. However, weights for the outermost shell were determined on the assumption that the gas density follows the same power law as the undisturbed gas in the shock model ($\rho \propto r^{-1.82}$) from the inside edge of that shell to infinity, thus allowing for the remainder of the cluster. Gas density is determined from the XSPEC norm of each model component, assuming that the gas density is constant in the corresponding shell. For the outermost shell, the gas density is determined at the center of the shell, under the assumptions used to determine the weights for that shell.

Even with 4000 counts per spectrum, the errors for the deprojected temperatures ($\sim$1 keV) are too large to reveal the temperature jump of the shock. For a shock Mach number of 1.2, the temperature jumps by $\sim$20% at the shock, but it falls rapidly behind the shock due to adiabatic expansion. As a result, the temperature rise in the shell immediately inside the shock is only expected to be $\sim$10%. The preshock temperature determined from the deprojection is approximately 4 keV, and we use this value for further calculations.

The deprojected electron density profile is shown in Figure 4. Electron densities are determined much more accurately than temperatures, chiefly because the overall *Chandra* count rate is insensitive to gas temperature in the range of interest. The density jump due to the shock at a radius of 211 kpc can be seen clearly. It is consistent with the $\sim$30% jump expected for a Mach 1.2 shock.

Using the deprojected temperature and density of the unshocked gas to normalize the physical parameters of the shock model, we find that the age of the outburst is $t_s = 1.4 \times 10^8$ yr and its total energy is $E_s = 9 \times 10^{60}$ ergs. The main source of uncertainty in the age of the shock is the preshock temperature, since the Mach number is not sensitive to the model (if the shocked cocoon is axially symmetric, the size we measure is not affected by projection). Shock energy is proportional to the preshock temperature. It also depends on the density profile of the unshocked gas. There is a substantial geometric uncertainty, since the shock front is clearly aspherical. Our estimate uses the part of the shock that is nearest to the cluster center, underestimating the total shocked volume, so tending to underestimate the total energy. Last, our estimate is affected by the inaccurate assumption of a point explosion. Despite all this, we expect the true energy of the outburst to be no more than a factor of $\sim$2 astray. The mean mechanical power of the outburst is $P_s = E_s/t_s \simeq 2 \times 10^{45}$ ergs s^{-1}.

4.4. *Shock versus Cold Front*

Interpreting the shock feature as a cold front instead would be difficult, although temperatures are not determined accurately enough from the current data to categorically rule this out. The density discontinuity (Fig. 4) shows that there is a front. If it is a cold front, the pressure must be continuous there. Otherwise the only physically reasonable interpretation is that it is a shock. For a density decrease $\sim$30%, the temperature must increase by $\sim$30% to keep the pressure continuous. Figure 5 shows projected temperature versus radius for the sector where the deprojection was done. Temperatures were obtained by fitting absorbed MEKAL models, with the absorbing column fixed at the foreground value ($N_{\rm H} = 4.94 \times 10^{20}$ cm^{-2}) and the abundance free. If anything, temperature decreases with radius at the front ($r =$ 211 kpc). The same is true at other P.A.s, where greater density steps would require greater temperature steps. According to the shock model, the maximum rise in projected temperature should be $\sim$5%, confined to the two rings behind the shock. This is consistent with Figure 5, although there is a mild negative temperature gradient in the vicinity of the shock that is not included in our simple shock model. The association between the front and the radio lobes is much better explained by a shock driven by an outburst than by a cold front. Furthermore, cold fronts are thought to be contact discontinuities formed when a body of gas moves through gas of higher entropy. In that case, it would be difficult to form a closed cold front, although this may just be possible for a cool core moving along our line of sight. By contrast, a shock

driven by an outburst at the cluster center is expected to surround the AGN. Altogether, the evidence strongly favors interpretation of this feature as a shock front.

5. DISCUSSION

5.1. *Jet History*

X-ray measurements of shock properties provide a new tool for the study of AGN outbursts and radio sources. The spherical explosion model used here to determine the age and energy of the AGN outburst in Hydra A is a very crude approximation to more realistic models (e.g., Heinz et al. 1998; Reynolds et al. 2001; Krause 2004). Nevertheless, it gives a reasonably accurate age and a good first approximation for the energy of the outburst. As discussed above, the $\sim$15% uncertainty in the age of the outburst is mainly due to uncertainty in the preshock temperature. More sophisticated modeling will constrain the history of the AGN outburst as well. The two main sinks for jet power may be regarded as the enthalpy of the radio plasma and the energy driving the shock. If a radio lobe is inflated slowly by a jet, so that its expansion into the surrounding gas is subsonic, the bulk of the jet power becomes the enthalpy of the radio plasma. If the lobe is inflated more quickly, it becomes overpressured relative to its surroundings and drives a shock into them. The overpressured lobe expands as it drives the shock, losing enthalpy in the process. Thus, the division of the total power between the energy driving the shock and the enthalpy of the radio plasma is determined by the overpressure of the radio lobes, which is determined mainly by the jet power. When shocks and cavities are both detected, both energies are accessible via X-ray observations. As a result, comparing more realistic models to the data will enable us to constrain the history of the outburst.

Although there are two X-ray cavities visible along the northeastern radio jet, none is evident at the location of the northern radio lobe. However, the surface brightness is low there and has structure on the scale of the lobe (including the shock front) that helps to mask any cavity if it is present. As found for the inner cavities (Nulsen et al. 2002), cavity C in the northeast is easier to recognize because of the bright rim along its outer edge (Fig. 1). Without this, the contrast of cavity C would only be $\sim$10%, making it considerably harder to see.

As noted above (§ 4.2), the proximity of the shock to the northern radio lobe argues that it is still being driven by that lobe. The shock jump conditions require that the lobe is overpressured by a factor $\sim$2 with respect to the unshocked gas. Unless it being refilled by the jets, the lobe would only expand by 15%–20% in radius, depending on its equation of state ($\gamma = 5/3$ or 4/3 for the values quoted), before coming to local pressure equilibrium. If the jets have ceased to refill the lobes, this source has been caught in a transient phase, while the lobes remain appreciably overpressured. We note that the equipartition pressure of the lobe, $\sim 1.3 \times 10^{-12}$ ergs cm^{-3} (Taylor et al. 1990), is an order of magnitude smaller than the surrounding gas pressure (David et al. 2001), typical of such sources.

The structure of the northeastern jet and the shock front suggest a complex history for the radio source. The sound speed in the radio plasma is expected to be a lot greater than that in the ambient ICM and comparable to the speed of light if the radio plasma is truly relativistic. In considering the dynamics of an outburst, we may regard pressure disturbances as propagating almost instantaneously throughout this medium. Thus, if the bulk of the northeastern jet was filled with a connected body of radio plasma at the onset of the current outburst, a compression wave (shock) would have been launched almost simultaneously from the whole of its length. The shock would then be strongest in the regions of lowest preshock pressure, near to the outer lobes, so that the shock front would have propagated further from the lobes than from the AGN. This would form a pinched waist around the AGN, between the lobes (see the simulations of Ruszkowski et al. 2004). Since the observed shock front bulges to the east and west of the AGN instead, there could not have been a connected body of radio plasma at the time that the jet was launched.

At the other extreme, with no preexisting radio plasma along the path of the jet, the outburst would have launched a jet that penetrated $\sim$300 kpc from the AGN to the northern radio lobe in $\sim 1.4 \times 10^8$ yr, with a mean speed of $v_j \simeq 2100$ km s^{-1} (or more, after allowing for projection effects). The bend in the jet at cavity C may be exaggerated by projection, but the real bend is unlikely to be small, since the jets are not tilted a long way from the plane of the sky (Taylor & Perley 1993; Lane et al. 2004). Therefore, jet momentum is probably not significant for the propagation of the jet beyond cavity C. In that case, the mean speed of the lobe would be excessive for a bubble that was driven most of the way by buoyancy (e.g., Churazov et al. 2001). Between these extremes, the jet may have been partly assisted along the trail of an older jet. For example, the jet may have been momentum driven to cavity C, beyond which it propagated through the trail left by an older outburst. The orientation of the old trail is affected by buoyancy and also by gas motions in the ICM. Thus, the asymmetry between the northern and southern jets can be the result of relatively modest asymmetries in the ICM.

5.2. *Cooling Flow Feedback and Preheating*

It needs to be asked whether the outburst in Hydra A has any connection to the cooling flow. If so, then the gas that fuels it must be cooled or cooling ICM. The line-emitting gas at the center of Hydra A might have been deposited by a merger (McNamara 1995), which could also be the source of fuel for the outburst. As discussed in § 1, the strongest argument for a connection between the outburst and the cooling flow is the difficulty of maintaining cool cores without feedback, but this does not rule out occasional mergers leading to larger than usual outbursts. On the other hand, large outbursts appear to play a significant role in balancing radiative losses (see below). In that case, it would be surprising if they were not part of the feedback process. The correlation between cooling luminosity and cavity heating power found by Birzan et al. (2004) also suggests strongly that the two are connected by feedback across the full range of systems. The outburst in Hydra A is 3 orders of magnitude more energetic than that which produced the 14 kpc shock in M87 ($\sim 10^{58}$ ergs; Forman et al. 2005). The outbursts responsible for the ripples in Perseus (Fabian et al. 2003) lie somewhere between these in energy. MS 0735.6+7421 (McNamara et al. 2005) and Hercules A (Nulsen et al. 2005) both have more energetic outbursts than Hydra A. At the least, outbursts span a large range of energies. A large sample is required to determine whether the large outbursts form a distinct class from those required to regulate cooling cores.

In the absence of heat sources, radiating gas cools to low temperature in approximately 1 cooling time, even after allowing for flow induced by the cooling. Thus, if the mass of gas inside radius r is $M_g(r)$ and the cooling time of gas at radius r is $t_c(r)$, a good approximation to the cooling rate when the gas between r_1 and r_2 is cooling to low temperatures is

$$\dot{M} \simeq \frac{M_g(r_2) - M_g(r_1)}{t_c(r_2) - t_c(r_1)}$$

(Fabian & Nulsen 1979). Applying this to the results of David et al. (2001) for Hydra A shows that the cooling rate would reach 100 $M_\odot$ yr^{-1} almost immediately at the onset of cooling and climb steadily thereafter. Such high cooling rates have yet to be demonstrated convincingly for any cluster (e.g., Peterson et al. 2003) and so must be rare. This requires that, if there is any period when the gas cools to low temperatures, it must be brief compared to observed central cooling times. Thus, another outburst must occur before or very soon after the central gas begins to cool in $\sim 4 \times 10^8$ yr (David et al. 2001). The maximum time between the last outburst and the next is therefore $t_{\rm max} \sim 5 \times 10^8$ yr, and the minimum average power required for such outbursts to prevent the gas from cooling is $P_{\rm min} \simeq E_s/t_{\rm min} \simeq 6 \times 10^{44}$ ergs s^{-1}, significantly more than the 2.5×10^{44} ergs s^{-1} radiated from within 150 kpc of the cluster center (David et al. 2001). The outburst in Hydra A cannot be a very efficient process for regulating the cool core. The shock front and outer radio lobe already lie outside the cooling flow region, "wasting" energy in the cluster at large radii and making the inefficiency manifest. Energy that is deposited outside the cooling flow region adds to the total energy of the ICM and, as noted by David et al. (2001), it can make an appreciable contribution to cluster "preheating." For a cluster temperature of 4 keV, the virial mass of Hydra A is about 5.4×10^{14} $M_\odot$ (Bryan & Norman 1998) and its gas mass is about 7.6×10^{13} $M_\odot$ (for a gas fraction of 14%). The mean heating power required to add 1 keV per particle to this gas over 10^{10} yr is 8×10^{44} ergs s^{-1}. Our estimates of the mean heating power from AGN outbursts lie in the range 6×10^{44}–2×10^{45} ergs s^{-1}, so the "waste" power could easily be a major source of preheating in Hydra A. There is no reason to believe that outbursts in much smaller systems (e.g., Finoguenov & Jones 2001) are more efficient, so these may also make significant contributions to preheating.

Birzan et al. (2004) found that bubble heating alone is insufficient to make up for radiative losses in most cooling flows. It should be noted that Hydra A was one of the exceptions. The total pV for the two 1.4 GHz inner cavities in Hydra A is 1.7×10^{59} ergs (Birzan et al. 2004). Taking the pressure from David et al. (2001), for cavity C to the northeast, we estimate $pV \simeq 3.7 \times 10^{59}$ ergs. Doubling this to allow for outer cavities to the southwest, the total pV for cavities in Hydra A is now $\sim 9 \times 10^{59}$ ergs. If the cavities are filled with relativistic plasma, their total enthalpy is the sum of $4pV$ for each, roughly one-third the estimated total energy of the shock. If it is devoid of X-ray–emitting gas, the enthalpy of the northern radio lobe would be similar to that of cavity C. The shocks in Hydra A and other systems (Fabian et al. 2003; Forman et al. 2005) show that bubble enthalpy may not be the most significant form of mechanical energy produced by AGN outbursts. As noted above, two systems have been found with even more energetic shocks, MS 0735.6+7421 (McNamara et al. 2005) and Hercules A (Nulsen et al. 2005). If they are a general feature of AGN outbursts, shocks will certainly help to account for the energetics of cooling flows. Birzan et al. (2004) found a large scatter in the ratio of radio power to bubble power, suggesting that current radio power is not a good measure of the history of AGN outbursts, even on timescales $\sim 10^7$–10^8 yr. However, while the central galaxies in cooling flow clusters are frequently active in the radio, radio sources as large as Hydra A are exceptional. If such outbursts do occur in a significant proportion of all clusters, they can be powerful radio sources for only a relatively small fraction of the time.

5.3. *Black Hole Growth*

The mass, M_s, that was accreted by the AGN to fuel this outburst can be related to the shock energy by $E_s = \epsilon M_s c^2$, where ϵ is the efficiency of the AGN for converting accreted mass into jet power (or other mechanical output). With our value for the shock energy, this gives $M_s \simeq 5 \times 10^6 \epsilon^{-1}$ $M_\odot$. This relationship between M_s and ϵ gives a value for M_s that exceeds the estimated mass of the black hole in Hydra A, $M_h \simeq 4 \times 10^9$ $M_\odot$ (Sambruna et al. 2000), unless the mechanical efficiency of the AGN $\epsilon \gtrsim 10^{-3}$. The mean mechanical power of the outburst, $P_s \simeq 2 \times 10^{45}$ ergs s^{-1}, is in the range of quasar luminosities but is a modest fraction of the Eddington limit for such a massive black hole. It is well in excess of the power needed to make up for radiative losses from the cooling flow.

6. CONCLUSION

A deep *Chandra* X-ray image of Hydra A has revealed new structure associated with the Hydra A radio source. This includes a break in the surface brightness 200–300 kpc from the cluster center that we interpret as a shock front. The shock front surrounds the low-frequency radio lobes, closely in places, showing a significant resemblance, and we interpret it as the cocoon shock of the radio source.

The Mach number of the shock varies in the range $\sim$1.2–1.4 around the front. Simple modeling shows that the shock outburst commenced $\sim 1.4 \times 10^8$ yr ago and that its energy $\sim 9 \times 10^{60}$ ergs. The mean mechanical power of the outburst $\sim 2 \times 10^{45}$ ergs s^{-1}, in the range of quasar luminosities. Such large outbursts can easily account for the radiative losses from the cooling flow in Hydra A. If they are part of a feedback cycle that sustains the cool gas in Hydra A, then the feedback heating process is inefficient, in the sense that more than half the mechanical energy output of the AGN is deposited in regions outside the cooling flow. Over time this would have produced significant "preheating" of Hydra A.

We thank Maxim Markevitch for drawing our attention to the shock feature before the new data were taken. We gratefully acknowledge the assistance of Alexey Vikhlinin and Maxim Markevitch in reducing the *Chandra* data. We thank Wendy Lane Peters and Namir Kassim for providing the radio map. We thank the referee for suggesting improvements to the paper. P. E. J. N. was partly supported by NASA grants NAS8-01130 and NAS8-03060. B. R. M. acknowledges support from NASA Long Term Space Astrophysics grant NAG5-11025, Chandra Guest Observer grant GO4-5146A, and contract 81305-001-034V from the Department of Energy through the Los Alamos National Laboratory.

REFERENCES

Birzan, L., Rafferty, D. A., McNamara, B. R., Wise, M. W., & Nulsen, P. E. J. 2004, ApJ, 607, 800
Blanton, E. L., Sarazin, C. L., McNamara, B. R., & Wise, M. W. 2001, ApJ, 558, L15
Böhringer, H., & Morfill, G. E. 1988, ApJ, 330, 609
Böhringer, H., Voges, W., Fabian, A. C., Edge, A. C., & Neumann, D. M. 1993, MNRAS, 264, L25
Bryan, G. L., & Norman, M. L. 1998, ApJ, 495, 80
Burns, J. O. 1990, AJ, 99, 14
Carilli, C. L., Perley, R. A., & Harris, D. E. 1994, MNRAS, 270, 173

Churazov, E., Brüggen, M., Kaiser, C. R., Böhringer, H., & Forman, W. 2001, ApJ, 554, 261
Churazov, E., Sunyaev, R., Forman, W., & Böhringer, H. 2002, MNRAS, 332, 729
Ciotti, L., & Ostriker, J. P. 2001, ApJ, 551, 131
David, L. P., Nulsen, P. E. J., McNamara, B. R., Forman, W., Jones, C., Ponman, T., Robertson, B., & Wise, M. 2001, ApJ, 557, 546
Fabian, A. C. 1994, ARA&A, 32, 277
Fabian, A. C., Mushotzky, R. F., Nulsen, P. E. J., & Peterson, J. R. 2001, MNRAS, 321, L20
Fabian, A. C., & Nulsen, P. E. J. 1979, MNRAS, 186, 783
Fabian, A. C., Sanders, J. S., Allen, S. W., Crawford, C. S., Iwasawa, K., Johnstone, R. M., Schmidt, R. W., & Taylor, G. B. 2003, MNRAS, 344, L43
Fabian, A. C., et al. 2000, MNRAS, 318, L65
Finoguenov, A., & Jones, C. 2001, ApJ, 547, L107
Forman, W., David, L., Jones, C., Markevitch, M., McNamara, B., & Vikhlinin, A. 2000, in Constructing the Universe with Clusters of Galaxies, ed. F. Durret & D. Gerbal (Paris: IAP)
Forman, W., et al. 2005, ApJ, in press (astro-ph/0312576)
Heinz, S., Choi, Y.-Y., Reynolds, C. S., & Begelman, M. C. 2002, ApJ, 569, L79
Heinz, S., Reynolds, C. S., & Begelman, M. C. 1998, ApJ, 501, 126
Kaastra, J. S., et al. 2004, A&A, 413, 415
Kraft, R. P., Forman, W. R., Churazov, E., Laslo, N., Jones, C., Markevitch, M., Murray, S. S., & Vikhlinin, A. 2004, ApJ, 601, 221
Kraft, R. P., Vázquez, S. E., Forman, W. R., Jones, C., Murray, S. S., Hardcastle, M. J., Worrall, D. M., & Churazov, E. 2003, ApJ, 592, 129
Krause, M. G. H. 2004, Ap&SS, 293, 255
Lane, W. M., Clarke, T. E., Taylor, G. B., Perley, R. A., & Kassim, N. E. 2004, AJ, 127, 48
Markevitch, M., Vikhlinin, A., & Forman, W. R. 2003, in ASP Conf. Ser. 301, Matter and Energy in Clusters of Galaxies, ed. S. Bowyer & C.-Y. Hwang (San Francisco: ASP), 37
McNamara, B. R. 1995, ApJ, 443, 77
McNamara, B. R., Nulsen, P. E. J., Wise, M. W., Rafferty, D. A., Carilli, C., Sarazin, C. L., & Blanton, E. L. 2005, Nature, 433, 45
McNamara, B. R., et al. 2000, ApJ, 534, L135
———. 2001, ApJ, 562, L149
Motl, P. M., Burns, J. O., Loken, C., Norman, M. L., & Bryan, G. 2004, ApJ, 606, 635
Narayan, R., & Medvedev, M. V. 2001, ApJ, 562, L129
Nulsen, P. E. J., David, L. P., McNamara, B. R., Jones, C., Forman, W. R., & Wise, M. 2002, ApJ, 568, 163
Nulsen, P. E. J., Hambrick, D. C., McNamara, B. R., Rafferty, D. A., Birzan, L., Wise, M. W., & David, L. P. 2005, ApJ, 625, L9
Peterson, J. R., Kahn, S. M., Paerels, F. B. S., Kaastra, J. S., Tamura, T., Bleeker, J. A. M., Ferrigno, C., & Jernigan, J. G. 2003, ApJ, 590, 207
Peterson, J. R., et al. 2001, A&A, 365, L104
Reynolds, C. S., Heinz, S., & Begelman, M. C. 2001, ApJ, 549, L179
Ruszkowski, M., Brüggen, M., & Begelman, M. C. 2004, ApJ, 611, 158
Sambruna, R. M., Chartas, G., Eracleous, M., Mushotzky, R. F., & Nousek, J. A. 2000, ApJ, 532, L91
Scheuer, P. A. G. 1974, MNRAS, 166, 513
Schindler, S., Castillo-Morales, A., De Fillippis, E., Schwope, A., & Wambganss, J. 2001, A&A, 376, L27
Tabor, G., & Binney, J. 1993, MNRAS, 263, 323
Tamura, T., et al. 2001, A&A, 365, L87
Taylor, G. B., & Perley, R. A. 1993, ApJ, 416, 554
Taylor, G. B., Perley, R. A., Inoue, M., Kato, T., Tabara, H., & Aizu, K. 1990, ApJ, 360, 41
Tucker, W., & David, L. P. 1997, ApJ, 484, 602
Young, A. J., Wilson, A. S., & Mundell, C. G. 2002, ApJ, 579, 560